Progress in Natural Science: Materials International xxx (xxxx) xxx–xxx

HOSTED BY

ELSEVIER

Contents lists available at ScienceDirect

Progress in Natural Science: Materials International

journal homepage: www.elsevier.com/locate/pnsmi

Original Research

The role of isotropic and anisotropic Hubbard corrections for the magnetic ordering and absolute band alignment of hematite α-Fe_2O_3(0001) surfaces

Sateesh Bandaru[a,b], Ivan Scivetti[c,d], Chi-Yung Yam[b,*], Gilberto Teobaldi[b,c,d]

[a] School of Chemical and Bioprocess Engineering, University College Dublin, 4 Dublin, Ireland
[b] Beijing Computational Science Research Center, Beijing, 100084, China
[c] Stephenson Institute for Renewable Energy, Department of Chemistry, The University of Liverpool, L69 3BX, Liverpool, United Kingdom
[d] Scientific Computing Department, Science and Technology Facilities Council, Daresbury Laboratory, WA4 4AD, Warrington, United Kingdom

ARTICLE INFO

Keywords:
Hematite
α-Fe_2O_3
Surfaces
Photo-electrodes
Density functional theory
Electronic properties
Magnetic properties

ABSTRACT

An isotropic (+U) and anisotropic [+(U−J)] corrected Density Functional Theory study for bulk hematite (α-Fe_2O_3) was carried out, and several competing terminations of its (0001) surface modeled via slabs of increasing thickness from twelve to thirty-six Fe-layers. In spite of small quantitative differences, the use of either U or (U-J) corrections showed not to qualitatively affect the results of the simulations both for bulk α-Fe_2O_3 and the lowest-energy α-Fe_2O_3(0001) surface studied, regardless of the thickness of the slab used. The energy favored anti-ferromagnetic ordering of bulk α-Fe_2O_3 was preserved in the relaxed slabs, with the largest surface-induced effects limited to the outermost three Fe-layers in the slabs. Mixed O- and Fe-terminations were found to be energetically favored and insulating. Conversely, fully O- or Fe-terminated surfaces were calculated to be energetically disfavored and metallic. Finally, the role of Fe- or O- termination for the semiconducting or metallic nature as well as absolute band alignment of α-Fe_2O_3(0001) surfaces was analyzed and discussed with respect to the challenges in enhancing the activity of α-Fe_2O_3 samples as photo-electrode for water splitting.

1. Introduction

Hematite α-Fe_2O_3 is the most common polymorph of iron oxide [1]. Hematite attracts considerable interest for a variety of applications in fields as diverse as heterogonous catalysis [2], nonlinear optics [3], lithium-ion batteries [4–6], gas sensing [7–10] and as photo-electrode for solar energy applications [1,11–19]. Experimentally, the optical bang-gap **(BG)** of α-Fe_2O_3 is roughly 2 eV [1,11–19], which makes the substrate capable of absorbing visible light. Furthermore, the energy alignment of the Valence Band **(VB)** and Conduction Band **(CB)** edges of hematite is compatible with both photo-reduction and photo-oxidation of liquid water H_2O [1,11–19]. Yet, owing to an unfavorable redox kinetics [1,11–19], photo-activated H_2O splitting by α-Fe_2O_3 requires the application of a 0.8–1.0 V (with respect to the normal hydrogen electrode) over-potential. To overcome this limitation, intense experimental efforts have been devoted to understanding α-Fe_2O_3 and its interfaces with H_2O [1,11–20]. Driven by the interest in improving the performance of α-Fe_2O_3 as photo-electrode for the water-splitting reaction, the focus of the computational community has been shifted to the simulation of α-Fe_2O_3 interfaces with water-based electrolytes, achieving important atomistic insights into the subject [21–24].

However, due to the increased cost in modelling both the α-Fe_2O_3 substrate and sufficiently extended H_2O layers in the interface model, Density Functional Theory (DFT) based simulation of α-Fe_2O_3 electrochemical interfaces has been necessarily executed using α-Fe_2O_3 substrates models made of typically 12 Fe-layer Fe_2O_3(0001) slabs [21–24]. Critically, in spite of substantial computational work on the simulation of α-Fe_2O_3 surfaces [25–31], the role of the slab thickness in affecting the structural and electronic properties, magnetism included, of α-Fe_2O_3 surfaces appears to have been partially overlooked in the specialized literature. More specifically, to best of our knowledge, a systematic study of the role of the slab thickness for the electronic (absolute band alignment) and magnetic ordering of α-Fe_2O_3 slab is currently missing. Although the role of slab thickness has been previously considered in Ref. [32], the use of partial slab-relaxation, and the ensuing creation of artificial dipoles across the α-Fe_2O_3 slab with unavoidable biases on the band alignment, provide the first motivation for the present study.

In addition, the occurrence of correlated *3d* electrons on the Fe atoms of α-Fe_2O_3, and the presence of magnetic (anti-ferromagnetic) ordering in this material have long stimulated computational interest and generated an healthy debate on the best accuracy-viability

* Corresponding author.
E-mail addresses: yamcy@csrc.ac.cn (C.-Y. Yam), gilberto.teobaldi@stfc.ac.uk (G. Teobaldi).

https://doi.org/10.1016/j.pnsc.2019.05.010
Received 10 May 2019; Received in revised form 16 May 2019; Accepted 27 May 2019

compromises for the simulation of this system [25,26,33–40]. Consensus on the use of reduced Hartree-Fock exchange mixing (12%) in screened hybrid XC-functional as being optimal for improved description of bulk α-Fe_2O_3 electronic and optical properties appears to have been reached [40]. However, the substantial computational cost of such approach and its limited applicability to slab models of α-Fe_2O_3 surfaces prompt further work on the subject. Furthermore, in spite of reports on the non-negligible role of spherically averaged (U) or anisotropic (U-J) on-site corrections to *3d* electrons atoms in correlated oxides such as β-MnO_2 [41] and $LiMn_2O_4$ [42], this aspect is yet to be studied for α-Fe_2O_3 surfaces, which provides the second motivation to the present work.

Motivated by these elements, and to sustain further research in α-Fe_2O_3 and its interfaces, here we present an extended study of the role of i) isotropic (U) and anisotropic (U-J) Hubbard corrections, and ii) slab thickness, for the DFT simulation of energy, electronic and magnetic properties of both bulk α-Fe_2O_3 and different terminations of the α-Fe_2O_3(0001) surfaces. Besides filling specialist gaps in the computational literature on α-Fe_2O_3, the present study provides, to the best of our knowledge for the first time, a comparison between the vacuum-aligned band edges for differently terminated α-Fe_2O_3(0001) surfaces. We believe these results to be relevant and informative also for the diversified communities with interest in band-engineering of hematite surfaces via molecular functionalization [11–24].

2. Computational details

All the simulation presented in this study were spin-polarized and carried out within the projector augmented wave (PAW) formalism implemented in the VASP program [43,44]. Semi-core states were included in the valence description of Fe-atoms. Prompted by their use in the computational literature on α-Fe_2O_3, two different semi-local approximations to the exchange-correlation (XC) functional were used: PW91 [45] (with Vosko interpolation [46] and PBE [47]. Hubbard corrections were applied to Fe atoms to improve the description of their correlated *3d* electrons. Hubbard corrections were applied following two schemes. In the first case, we used the original anisotropic (U-J) approach first proposed by Liechtenstein et al. [48,49], with Coulomb U = 5 eV and screened exchange J = 1 eV parameters. In the second case we used the isotopically averaged formulation of Dudarev et al. [50,51], with an effective U_{eff} = U-J = 4 eV correction (U from now onwards). As previously noted, this choice was prompted by reports on non-negligible deviations between U and (U-J) results for other correlated oxides [41,42] and the lack of results on the matter for α-Fe_2O_3 surfaces.

In all cases, the plane-wave cutoff was set to 550 eV and geometry optimization were converged using a force threshold of 10^{-2} eV/Å. For the surface calculations, a vacuum buffer of at least 15 Å was present between replicated images of the slabs. All the atoms in the slabs were relaxed, maintaining the symmetry point-group of their initial bulk-like positions. For geometry optimization, Brillouin zone sampling was performed on the basis of Monkhorst-Pack [52] grids of 8 × 8 × 8 (bulk) and 4 × 4 × 1 (surfaces). Finer 8 × 8 × 1 grids were used for the electronic characterization of the surfaces.

Following established procedures [25,53–55], and assuming thermodynamic equilibrium between Fe and O atoms as well as corresponding reservoirs, the surface energy of the studied *symmetric* slab (γ) was calculated as a function of the chemical potential of the oxygen atoms (μ_O) via the following equation:

$$\gamma = \frac{1}{2A}\left[E^{slab}_{Fe_2O_3} - \frac{1}{2}N_{Fe}\mu^{bulk}_{Fe_2O_3} + \left(\frac{3}{2}N_{Fe} - N_O\right)\mu_O\right]$$

where A is slab surface area. $E^{slab}_{Fe_2O_3}$ is the total energy of the slab comprising N_{Fe}Fe-atoms and N_OO-atoms. $\mu^{bulk}_{Fe_2O_3}$ is the chemical potential of hematite α-Fe_2O_3 bulk, as approximated by the corresponding DFT energy (per formula unit). As in Ref. [25], the chemical potential of oxygen (μ_O) was referenced to half of the total energy of an isolated (triplet) oxygen molecule, E_{O2}, leading to a relative oxygen chemical potential ($\Delta\mu_O$) defined as:

$$\Delta\mu_o = \mu_o - \frac{1}{2}E_{O_2}$$

which was used as independent variable in the plots for γ.

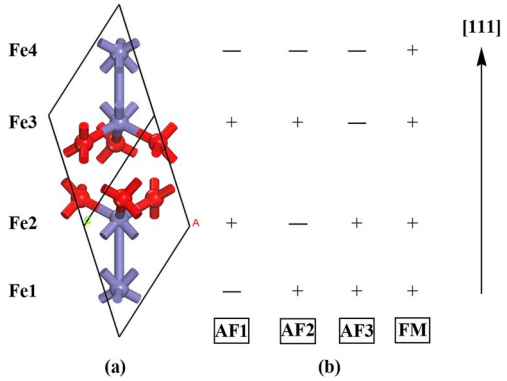

Fig. 1. (a) The adopted rhombohedral primitive cell for α-Fe_2O_3. (b) The considered anti-ferromagnetic (AF) ordering for the four Fe-atoms (Fe1 to Fe4) along the [111] direction. Fe: purple, O: red. Plus (+) and minus (−) marks refer to the sign of the atomic magnetic moments. For the adopted labeling, Fe1–Fe2 and Fe3–Fe4 distances are shorter than the Fe2–Fe3 one. (For interpretation of the references to color in this figure legend, the reader is referred to the Web version of this article.)

3. Results and discussion

3.1. Bulk α-Fe_2O_3

The investigation started considering the role of the adopted simulation protocol for the structural and magnetic properties of bulk hematite α-Fe_2O_3. Following a seminal DFT + U and DFT + (U-J) study of bulk α-Fe_2O_3 [33], a rhombohedral primitive cell was adopted for the simulations (Fig. 1). As in [33], we considered different magnetic ordering along the [111] direction, and explored in detail the role of the simulation protocol for the optimized structure as well as the relative energy of these magnetic solutions. Specifically, we focused on four possible magnetic orderings: besides the ferromagnetic **(FM)** solution, we also considered three competing anti-ferromagnetic **(AF)** orderings that differ in the pattern of the Fe magnetic moments along the [111] direction. Using plus (+) and minus (−) marks to indicate the positive or negative magnetic moment for Fe atoms in the Fe1–Fe4 series along the [111] direction (Fig. 1), the configurations studied are: **AF1** (- + + -), **AF2**(+ - + -), and **AF3**(+ + - -). As shown in Fig. 1, for the adopted rhombohedral representation of α-Fe_2O_3, different short (~2.9 Å) and long (~4.0 Å) distances exist between adjacent Fe atoms along the [111] direction.

For each magnetic ordering and simulation protocol considered, we next optimized the cell volume maintaining the rhombohedral symmetry (Figs. S1–S4 in the Supporting Information). Table 1 reports a summary of the optimized structural parameters, relative energies and total magnetic moment as a function of the simulation method used.

Regardless of the simulation protocol, the AF1 (- + + -) solution, with antiferromagnetic coupling between closest Fe-atoms in the structure (Fe1–Fe2 and Fe3–Fe4 in Fig. 1), is energetically favored, in accordance with earlier unscreened hybrid-DFT (B3LYP) results [56], relatively recent screened hybrid DFT (HSE06 with reduced 12% Hartree-Fock mixing) simulations [40], and experimental results [57].

Table 1
Calculated relative energy (ΔE, eV) and absolute value of the Fe-atom magnetic moment (M, μ_B) for the optimized cell of bulk α-Fe_2O_3, together with optimized volume per atom V (Å^3) and c/a ratio, as a function of the simulation protocol used. All the Fe-atoms in the simulation cell (Fig. 1) are calculated to have the same absolute value magnetic moment.

Magnetic Ordering	PBE + U				PBE + (U-J)			
	ΔE (eV)	M (μ_B)	V (Å^3)	c/a	ΔE (eV)	M (μ_B)	V (Å^3)	c/a
AF1 (- + + -)	0.0	4.151	10.31	2.74	0.0	4.145	10.32	2.74
AF2 (+ - + -)	1.66	4.224	10.41	2.72	1.68	4.219	10.43	2.72
AF3 (+ + - -)	1.12	4.201	10.39	2.70	1.10	4.193	10.40	2.70
FM (+ + + +)	3.22	4.318	10.58	2.71	3.22	4.310	10.53	2.71
MagneticOrdering	PW91 + U ΔE (eV)	M (μ_B)	V (Å^3)	c/a	PW91 + (U-J) ΔE (eV)	M (μ_B)	V (Å^3)	c/a
AF1 (- + + -)	0.0	4.142	10.29	2.73	0.0	4.136	10.29	2.74
AF2 (+ - + -)	1.66	4.214	10.42	2.72	1.68	4.210	10.39	2.72
AF3 (+ + - -)	1.15	4.193	10.36	2.70	1.13	4.186	10.35	2.69
FM (+ + + +)	3.19	4.310	10.48	2.71	3.19	4.304	10.53	2.71

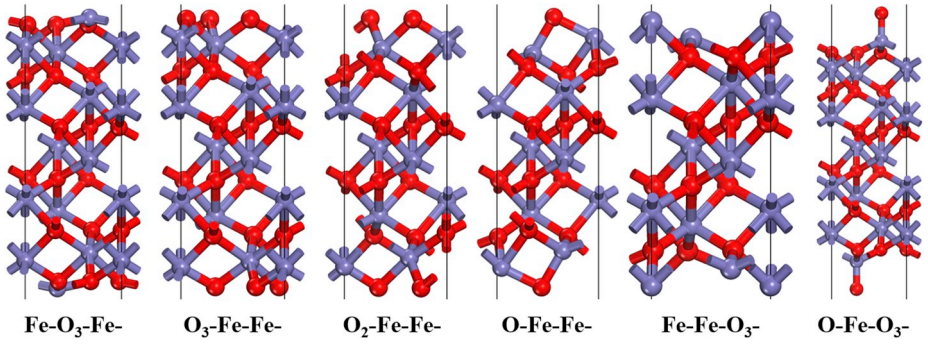

Fig. 2. Side-view of the different α-Fe_2O_3 (0001) terminations studied (12 Fe-layer slab, optimized geometry) with the corresponding labeling from Ref. [29]. Same atom color labeling as in Fig. 1. (For interpretation of the references to color in this figure legend, the reader is referred to the Web version of this article.)

Qualitatively, the use of isotropic (U) or anisotropic (U-J) corrections does not affect the relative energy of the different magnetic ordering consideration. The AF2(+- + -) solution is consistently calculated to have a noticeable higher energy (~1.1 eV/cell) than the AF1 (- + + -) ground state and with the AF3(+ + - -) solution being energetically disfavored by a further ~0.5 eV/cell. In all cases, and in agreement with earlier DFT-studies of bulk α-Fe_2O_3 [33], the FM solution is found to be energetically disfavored with respect to high-energy AF solutions by over 1 eV/cell, and up to over 3 eV/cell with respect to the AF1 (- + + -) ground state.

Irrespective of the use of U or (U-J) corrections and of the PBE or PW91 XC-functional, the optimized cell volume (V, Å^3) and c/a ratios for bulk α-Fe_2O_3 are found to deviate by less than 0.025 Å^3 (2.5%) and 0.01 (3.7%) from the experimental values for V (10.06 Å^3) and c/a (2.731) [58].

As also shown in Table 1, regardless the use of the U or (U-J) corrections, the calculated magnetic moments on the Fe-atoms for the AF1 (- + + -) ground state turn out to be weakly dependent (by less than 0.1 μ_B) on the use of U or (U-J) corrections. Notably, the calculated value of roughly 4.1 μ_B is in good agreement with earlier HSE06 results (4.16 μ_B regardless the use of 25% or 12% Hartree Fock mixing) [40], and thence underestimated by roughly 0.5 μ_B with respect to the experimental results in Ref. [58]. Although the similarity between the results for magnetic moments α-Fe_2O_3 from DFT + U approaches and HSE06 hybrid functional has been previously noted and discussed in Ref. [40], the present results indicate that the same conclusion holds also for anisotropic Hubbard corrections [DFT + (U-J)] as applied here (not considered in [40]).

Overall, these results indicate that in contrast to reports on other correlated oxides (such as β-MnO_2 [41] and $LiMn_2O_4$ [42]), the structural, energy and magnetic properties of bulk α-Fe_2O_3 are minimally affected by the use of isotropic (U) or anisotropic (U-J) Hubbard corrections. Whether these conclusions are held also for the surfaces of α-Fe_2O_3 will be explored in the next sections.

Finally, for the specialist reader, it is noted that while the present results on the energetic favorability of the AF1 (- + + -) solution agree with B3LYP [56] and HSE06 hybrid DFT results [40] as well as with experiments [40], they are at odds with earlier PW91 + U reports on the same system [33], where the AF3(+ + - -) solution was suggested to be energetically favored.

3.2. α-Fe_2O_3(0001) surface models

For the study of α-Fe_2O_3(0001) surfaces, we considered (hexagonal) symmetric slabs built from the optimized structure of the computed AF1 (- + + -) ground state (Section 3.1). All the initial slab structures contained at least one roto-inversion axis across the slab. To prevent the occurrence of artificial dipoles across the slab model, the initial point-group symmetry of the slab was maintained during the geometry optimizations. Fig. 2 reports the atomic structure of the 12 Fe-layer slab studied with the same labeling as in Ref. [29].

The surface terminations are briefly introduced as follows: the **Fe–O_3–Fe** termination is a stoichiometric truncation of the hexagonal α-Fe_2O_3bulk cell in the (0001) plane. The **O_3–Fe–Fe** surface stems from removal of one Fe-atoms from the **Fe–O_3–Fe** model, leading to a fully oxygen terminated surface. The removal of the additional O-atoms from this latter surface leads to the **O_2–Fe–Fe-** and **O–Fe–Fe** terminations. The complete removal of the topmost Fe and O atoms from the stoichiometric **O_3–Fe–Fe** surface leads to the **Fe–Fe–O_3-** model, for which a Fe-layer (not O-layer) is exposed to the vacuum. The addition of one O-atoms to the stoichiometric model **O_3–Fe–Fe** leads to the **O–Fe–O_3-** termination.

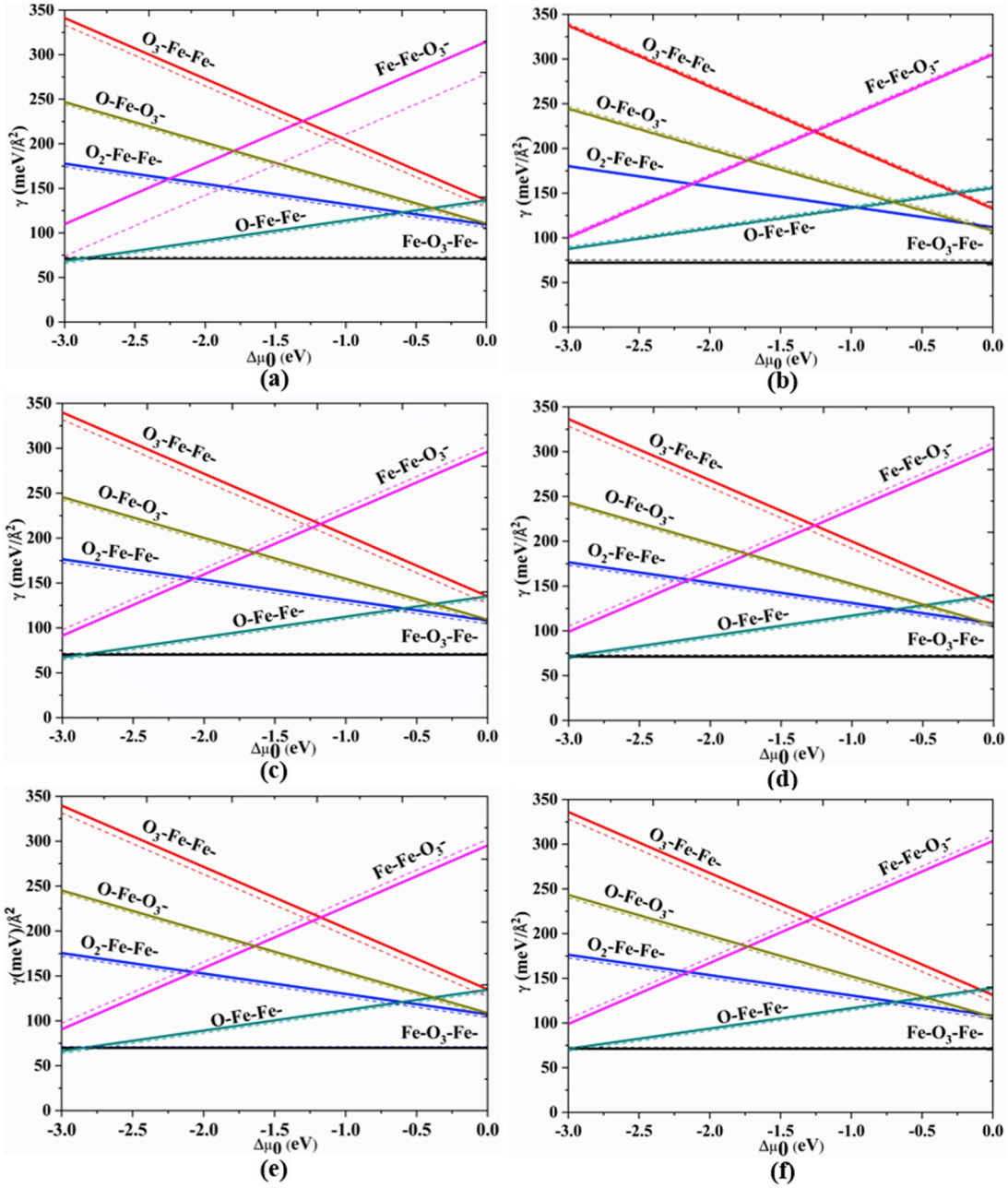

Fig. 3. Calculated surface energies (γ) as a function of the change in the chemical potential for the O-atoms with respect to their reference state ($\Delta\mu_O$, eV) for **(a)** 12 Fe-layer slab, PBE; **(b)** 12 Fe-layer slab, PW91; **(c)** 24 Fe-layer slab, PBE, **(d)** 24 Fe-layer slab, PW91; **(e)** 36 Fe-layer slab, PBE, **(f)** 36 Fe-layer slab, PW91. Continuous lines report the results for isotropic (U) corrections, dashed lines for anisotropic (U–J) corrections. O-poor (rich) conditions correspond to more (less) negative values of $\Delta\mu_O$. Same labeling for the surface models as in Fig. 2.

In spite of intense theoretical and computational research on α-Fe_2O_3 (0001) [25–31], to the best of our knowledge the convergence of the calculated magnetic and electronic properties with respect to thickness of the modeled, fully relaxed [32] slab has not been benchmarked in the available literature. Therefore, we expanded our study to consider also the thicker 24 Fe-layer (Fig. S5 in the Supporting Information) and 36 Fe-layer (Fig. S6) slabs besides the 12 Fe-layer models (Fig. 1). An additional motivation for this choice was the dependence of the optimized magnetic ordering on the slab thickness, previously experienced by some of the authors in modelling surfaces of correlated oxides (such as $LiMn_2O_4$ in [42]).

3.3. α-Fe_2O_3 (0001) surface energies

Given the different stoichiometry of the studied surface models, we used the calculated surface energy (γ) as a function of the change in chemical potential for the O atoms from its reference state ($\Delta\mu_O$, see Section 2) to analyze their relative energy. Fig. 3 reports the calculated results as a function of the computational protocol used and the slab thickness changing from 12 to 24 and 36 Fe-layers.

Based on the protocol used and consistent with earlier computational reports [25], the simulations predict that the stoichiometric **Fe–O_3–Fe** termination is energetically favored over the whole range of $\Delta\mu_O$ values modeled. This result holds regardless of the XC-functional

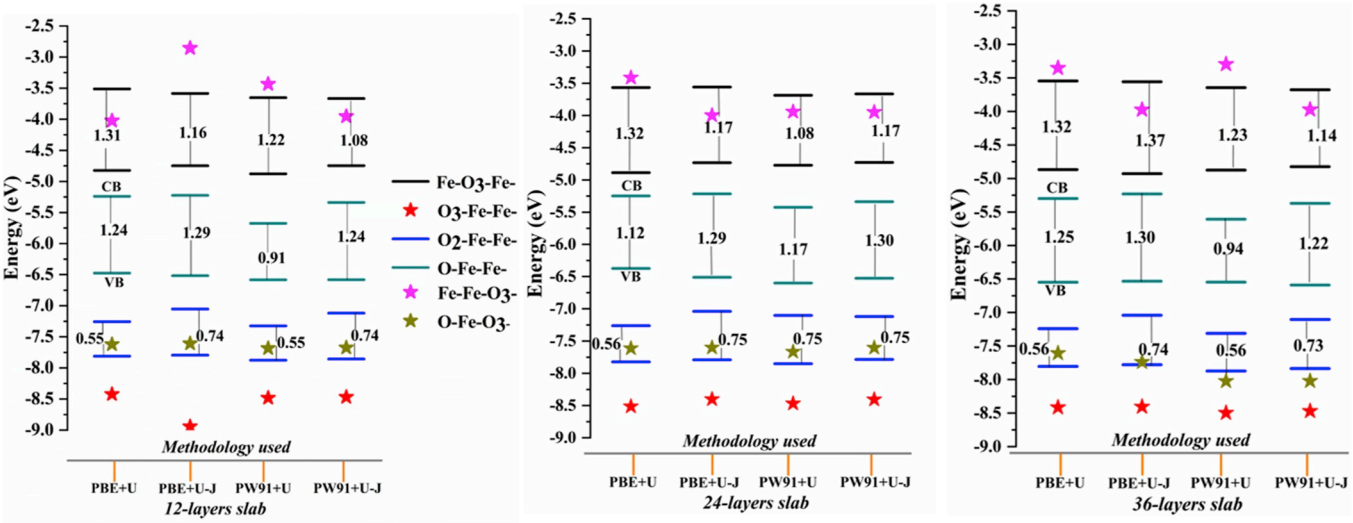

Fig. 4. Calculated vacuum aligned Valence and Conduction Band edges (horizontal lines) and corresponding band gap (eV) for the considered terminations of the α-Fe_2O_3 (0001) surface as a function of the simulation protocol and slab thickness. The calculated vacuum-aligned Fermi Energy of the metallic slabs is marked with stars.

used (PBE or PW91) and the application of isotropic (U) or anisotropic (U-J) Hubbard corrections to the Fe atoms. The close qualitative agreement between the results for 12, 24 and 36 Fe-layer slabs (see also Table S1 and Fig. S7 in the Supporting Information) suggests that, overall, the use of 12 Fe-layers slab is sufficient to qualitatively screen relative surface energies of different α-Fe_2O_3 (0001) surfaces. However, the results in Fig. 3 (and Table S1 in the Supporting Information) also reveal that thicker slabs (i.e. at least 24 Fe-layers slab) are needed to achieve quantitatively robust (< 2 meV/Å^2) convergence of the calculated surface energy for a given computational approach.

This analysis reveals also an important qualitative difference due to the use of isotropic (U) or anistropic (U-J) corrections. As shown in Fig. 3 (and Table S1 and Fig. S7 in the Supporting Information), at $\Delta\mu_O = 0$, the isotropically corrected PBE + U and PW91 + U simulation predicts the second-lowest γ for the **O_2–Fe–Fe** surface, and the third-lowest γ for the **O–Fe–O_3-** model. However, the relative energy ranking of these two terminations is inverted by application of anisotropic (U-J) corrections to both the PBE and PW91 simulations. That is, at PBE/PW91 + (U-J) level, the calculated γ for **O–Fe–O_3-** is now lower than for the **O_2–Fe–Fe-**surface. Thus, contrary to the bulk case, we find the energy ranking of higher energy α-Fe_2O_3 (0001) terminations to depend quantitatively and qualitatively on the application of isotropic and anisotropic corrections. The absence of hybrid DFT results on the relative energy of the different surface termination studied (Fig. 1) prevents us from further discussing these results against higher-level computational results. We nevertheless hope that these findings will stimulate further computational work in the subject.

We finally note that the PW91 + U values for the γ of the stoichiometric termination (**Fe–O_3–Fe-**in the present notation) computed in Ref. [25], using an AF3 magnetic ordering to prepare the slabs (not AF1 as here, see Section 3.1) and a reduced 350 eV plane-wave cutoff, is 105 meV/Å^2. Conversely, our PW91 + U value (for an AF1 initialized slab and a plane-wave cutoff of 550 eV) is 72.09 meV/Å^2 which is over 30 meV/Å^2 lower than that of in Ref. [25]. Therefore it may be considered that these results reinforce the fact that the AF1 ordering is energetically favored also for slabs.

3.4. α-Fe_2O_3 (0001) surface: magnetic properties

To analyze the dependence of the calculated magnetic properties on the slab-thickness, the total slab and atom-resolved magnetic moments are presented in Tables S2–S5 in the Supporting information. Starting from the total magnetic moment calculated for the slabs (Table S2), the simulations indicate that the AF1 magnetic ordering is consistently maintained also in the fully relaxed slabs. As a result, the total slab magnetic moment calculated for the stoichiometric **Fe–O_3–Fe** termination is 0 μ_B. Conversely, non-zero total magnetic moments are computed for the non-stoichiometric slabs. This trend turns out to be independent of changes in the XC-functional (i.e. PBE or PW91), and of the use of U or (U-J) corrections. In line with the results for the surface energy (Section 3.3), analysis of the total slab magnetic moment of the slab reiterates the limited quantitative convergence of the results for the 12 Fe-layer slab with respect to the 24 and 36 Fe-layer systems.

Analysis of the atomic magnetic moments as a function of the slab thickness (Tables S3–S5 in the Supporting Information) provides detailed insights into the role of surface relaxation for the slab magnetic properties. In general, and regardless of the computational protocol used, the under-coordination of the surface atoms and the overall slab relaxation does induce deviations in the atomic magnetic moments from the bulk value (~ 4.15 μ_B, as shown in Table 1). The larger changes from the bulk results (up to over 1 μ_B) are found to be localized on the three top-most Fe layers (Fe1 to Fe3 in Tables S3–S5), with substantially smaller (0.01 μ_B) changes present also for the innermost Fe-atoms as a function of the slab thickness. As previously observed for the surface energies (Section 3.3), the convergence of the magnetic moments of Fe atoms with respect to the slab thickness is found not to be absolute for 12 Fe-layer slabs. The deviations for the magnetic moments of the topmost Fe atoms in progressively thicker slabs are computed to be as large as ~ 0.2 μ_B.

3.5. α-Fe_2O_3 (0001) surface: absolute band alignment

Complementary with the previous analysis, absolute band edge alignments and BGs were analyzed as well as their dependence on the computational protocol used and the slab thickness.

The improvement of electronic conductivity for α-Fe_2O_3 surfaces by defect engineering is experimentally observed to benefit the photo-electro-catalytic properties of the substrate [20]. As the surfaces of correlated oxides can develop metallic surface states increasing the electronic conductivity [42,59], it is therefore relevant to investigate whether the different α-Fe_2O_3 (0001) terminations considered present metallic states and how their presence affects the surface energy. The outcome of such analysis is expected to positively contribute to the development of molecular functionalization strategies to realize α-Fe_2O_3 surfaces with enhanced electronic conductivity.

Fig. 4 shows the calculated absolute band-alignments with respect to the vacuum level (0 eV) and BGs for the considered surface models as

a function of the computational protocol used. Qualitatively, all of the computational approaches predict a non-zero BG for the **Fe–O_3–Fe-**, **O_2–Fe–Fe-** and **O–Fe–Fe** terminations and metallization (non-zero Density of States at the Fermi Energy) for the **O_3–Fe–Fe**, **Fe–Fe–O_3-** and **O–Fe–O_3-** terminations. The comparison between these results and the calculated surface energies (Fig. 3 and Table S1 in the Supporting Information) indicates that the occurrence of metallic states does not directly correlate with a higher surface energy. Although the **Fe–O_3–Fe-** surface (semiconducting) is energetically favored, the second lowest energy surfaces [**O_2–Fe–Fe-** or **O–Fe–O_3-** depending on the use of U or (U-J)] displays both a semiconducting (**O_2–Fe–Fe-**) and metallic (**O–Fe–O_3-**) nature.

Given the interest in engineering the VB-edge of α-Fe_2O_3 substrates to higher energy values closer to the redox potential of H_2O oxidation (required for enhanced photo-oxidation applications) [11–19], it is unfortunate to be observed that for all the surface terminations studied, only the very high energy (Fig. 3) **Fe–Fe–O_3-** termination fulfills such desirable requirement. However, as shown in Fig. 4, with a work-function in the 3.5–4.0 eV range, the calculated Fermi energy for **Fe–Fe–O_3-** can, depending on the simulation method, be up to over 1 eV higher in energy than the VB-edge of the energy-favored **Fe–O_3–Fe-** termination. The presence of under-coordinated surface of Fe-atoms in this model, suggests that the preparation of the surface in the presence of molecular species capable to coordinate the dangling bonds of the surface Fe-atoms (e.g. lone-pair bearing organic functional groups) may be meaningfully considered and explored, to bring the surface VB-edge (Fermi energy) higher in energy and closer to the redox potential of H_2O oxidation [11–19].

The observed dependence of the calculated BGs on the simulation protocol and slab thickness is rather weak with the deviations within 20–30 meV for all the terminations. The exception to this trend are the **Fe–O_3–Fe-** [60 meV at PW91 + (U-J) level], **O_2–Fe–Fe-** (120 meV at PBE + U level) and **O–Fe–Fe-** (up to nearly 300 meV from 12 to 24 to 36 Fe-layer slabs at PW91 + U level) terminations. Based on these results, the PBE + (U-J) approach emerges as the one capable of the best convergence between the results for 12, 24 and 36 Fe-layers slab. When considered against the expectedly large errors (over 1 eV for bulk α-Fe_2O_3 [40]) for the BGs due residual self-interaction errors in the simulations, the dependence of the BG-results on the slab thickness is however sufficiently contained to enable semi-quantitative characterization and comparison of the electronic properties of α-Fe_2O_3 (0001) surfaces. This conclusion in turn supports the previous use of such minimal model for the modelling of α-Fe_2O_3 (0001) interfaces with H_2O [21–24].

Finally, It is noted that in Ref. [25], for a 350 eV cut-off, all the surface terminations considered here were computed to be semiconducting (non-zero BG) at PW91 + U level. This is in contrast with the present case, and the metallic states (zero BG) calculated for the **O_3–Fe–Fe-**, **Fe–Fe–O_3-**, **O–Fe–O_3-** surfaces. These deviations are attributed to the different magnetic ordering (AF1 here, AF3 in [25]) used to initialize the slab relaxation.

4. Conclusions

An extensive study of the role of isotropic (U) or anisotropic (U-J) corrections has been carried out for the simulation of both bulk α-Fe_2O_3 and α-Fe_2O_3 (0001) surface with slabs of different thickness. Results indicate that, in spite of small quantitative differences, the energy, magnetic and electronic properties of α-Fe_2O_3 bulk and (0001) surfaces do not strongly depend on the use of U or (U-J) corrections. In all cases, it has been found that the energy favored anti-ferromagnetic ordering of bulk α-Fe_2O_3 is preserved also in the relaxed slabs, regardless of their thickness. For all the surface terminations, and regardless of the simulation protocol used, the surface relaxation mostly affects the magnetic properties of the three topmost Fe-layers, with the innermost layers maintaining bulk-like magnetic moments. Mixed O- and Fe-terminated surfaces are calculated to be energetically favored and semiconducting. Conversely, fully O- or Fe-terminated surfaces are computed to be both energetically disfavored and metallic. The calculated values of the work-function for such metallic surfaces suggest potentially favorable alignment with H_2O oxidation potential, inviting further research in their stabilization by molecular functionalization towards the enhancement of the performance of α-Fe_2O_3–based photo-anodes.

Acknowledgments

Sateesh Bandaru acknowledges gratefully the financial support of the Natural Science Foundation of China (No. 21650110464) and computational resources from the Beijing Computational Science Research Center. Gilberto Teobaldi acknowledges Associate Membership to the Beijing Computational Science Research Center, support from EPSRC UK (EP/I004483/1, EP/P022189/1, EP/P022189/2, and EP/P020194/1) and CoSeC at STFC. Ivan Scivetti acknowledges CCP5 funding and associated CoSeC support at STFC.

Appendix A. Supplementary data

Supplementary data to this article can be found online at https://doi.org/10.1016/j.pnsc.2019.05.010.

References

[1] L. Pauling, S.B. Hendricks, J. Am. Chem. Soc. 47 (1925) 781–790.
[2] W. Geus, Appl. Catal. 25 (1986) 313–333.
[3] T. Hashimoto, T. Yoko, S. Sakka, J. Ceram. Soc. Jpn. 101 (1993) 64–68.
[4] D.N. Srivastava, N. Perkas, A. Gedanken, I. Felner, J. Phys. Chem. B 106 (2002) 1878–1883.
[5] C. Feldmann, Adv. Mater. 13 (2001) 1301–1303.
[6] G. Jain, M. Balasubramanian, J.J. Xu, Chem. Mater. 18 (2006) 423–434.
[7] X.L. Gou, G.X. Wang, X.Y. Kong, D. Wexler, J. Horvat, J. Yang, J. Park, Chem. Eur. J14 (2008) 5996–6002.
[8] X. Li, W. Wei, S. Wang, L. Kuai, B. Geng, Nanoscale 3 (2011) 718–724.
[9] J. Ma, L. Mei, Y. Chen, Q. Li, T. Wang, Z. Xu, X. Duan, W. Zheng, Nanoscale 5 (2013) 895–898.
[10] J. Deng, J. Ma, L. Mei, Y. Tang, Y. Chen, T. Lv, Z. Xu, T. Wang, J. Mater. Chem. 1 (2013) 12400–12403.
[11] J. Kennedy, K. Freese, J. Electrochem. Soc. 125 (1978) 709–714.
[12] K. Sivula, F. Le Formal, M. Grätzel, Chem.Sus.Chem 4 (2011) 432–449.
[13] S.C. Warren, K. Voitchovsky, H. Dotan, C.M. Leroy, M. Cornuz, F. Stellacci, C. Hebert, A. Rotschild, M. Grätzel, Nat. Mater. 12 (2013) 842–849.
[14] A. Duret, M. Grätzel, J. Phys. Chem. B 109 (2005) 17184–17191.
[15] N. Beermann, L. Vayssieres, S.-E. Lindquist, A. Hagfeldt, J. Electrochem. Soc. 147 (2000) 2456–2461.
[16] G.K. Mor, H.E. Prakasam, O.K. Varghese, K. Shankar, C.A. Grimes, Nano Lett. 7 (2007) 2356–2364.
[17] T. Lopes, L. Andrade, H.A. Ribeiro, A. Mendes, Int. J. Hydrogen Energy 35 (2010) 11601–11608.
[18] M.A. Gondal, A. Hameed, Z.H. Yamani, A. Suwaiyan, Appl. Catal., A 268 (2004) 159–167.
[19] L.L. Hu, T. Yoko, H. Kozuka, S. Sakka, Thin Solid Films 219 (1982) 18–23.
[20] Y. Yang, M. Forster, Y. Ling, G. Wang, T. Zhai, Y. Tong, A.J. Cowan, Y. Li, Angew. Chem. Int. Ed. 55 (2016) 3403–3407.
[21] N.J. English, M. Rahman, N. Wadnerkar, J.M.D. MacElroy, Phys. Chem. Chem. Phys. 16 (2014) 14445–14454.
[22] G.F. von Rudorff, R. Jakobsen, K.M. Rosso, J. Blumberger, J. Phys. Condens. Matter 28 (2016) 394001.
[23] G.F. von Rudorff, R. Jakobsen, K.M. Rosso, J. Blumberger, J. Phys. Chem. Lett. 7 (2016) 1155–1160.
[24] K. Ulman, E. Poli, N. Seriani, S. Piccinin, R. Gebauer, J. Chem. Phys. 150 (2019) 041707.
[25] A. Rohrbach, J. Hafner, G. Kresse, Phys. Rev. B 70 (2004) 125426.
[26] P.L. Liao, E.A. Carter, Phys. Chem. Chem. Phys. 13 (2011) 15189–15199.
[27] K. Ulman, M.-T. Nguyen, N. Seriani, R. Gebauer, J. Chem. Phys. 144 (2016) 094701.
[28] K. Ulman, M.-T. Nguyen, N. Seriani, S. Piccinin, R. Gebauer, ACS Catal. 7 (2017) 1793–1804.
[29] M.-T. Nguyen, N. Seriani, S. Piccinin, R. Gebauer, J. Chem. Phys. 140 (2014) 064703.
[30] P. Liao, J.A. Keith, E.A. Carter, J. Am. Chem. Soc. 134 (2012) 13296–13309.
[31] M.-T. Nguyen, S. Piccinin, N. Seriani, R. Gebauer, ACS Catal. 5 (2015) 715–721.
[32] F. A-Ramírez, J.M.M. Magadan, J.R.B. Gomes, F. Illas, Surf. Sci. 558 (2004) 4–14.
[33] G. Rollmann, A. Rohrbach, P. Entel, J. Hafner, Phys. Rev. B 69 (2004) 165107.
[34] M.P.J. Punkkinen, K. Kokko, W. Hergert, I.J. Väyrynen, J. Phys. Condens. Matter 11

(1999) 2341–2349.
[35] L.M. Sandratskii, M. Uhl, J. Kübler, J. Phys. Condens. Matter 8 (1996) 983–989.
[36] T. Uozumi, K. Okada, A. Kotani, J. Electron. Spectrosc. Relat. Phenom. 78 (1996) 103–106.
[37] A. Fujimori, M. Saeki, N. Kimizuka, M. Taniguchi, M. Suga, Phys. Rev. B 39 (1989) 13 478.
[38] F. Ciccacci, L. Braicovich, E. Puppin, E. Vescovo, Phys. Rev. B 44 (1991) 10444.
[39] M. Catti, G. Valerio, R. Dovesi, Phys. Rev. B 51 (1995) 7441.
[40] Z.D. Pozun, G. Henkelman, J. Chem. Phys. 134 (2011) 224706.
[41] D.A. Tompsett, D.S. Middlemiss, M.S. Islam, Phys. Rev. B 86 (2012) 205126.
[42] I. Scivetti, G. Teobaldi, J. Phys. Chem. C 119 (2015) 21358–21368.
[43] G. Kresse, J. Furthmuller, Phys. Rev. B 54 (1996) 11169.
[44] G. Kresse, J. Furthmuller, Comput. Mater. Sci. 6 (1996) 15–50.
[45] J. Perdew, J. Chevary, S. Vosko, K. Jackson, M. Pederson, D. Singh, C. Fiolhais, Phys. Rev. B 46 (1992) 6671.
[46] S.H. Vosko, L. Wilk, M. Nusair, Can. J. Phys. 58 (1980) 1200–1211.
[47] J.P. Perdew, K. Burke, M. Ernzerhof, Phys. Rev. Lett. 77 (1996) 3865–3868.
[48] I. Liechtenstein, V.I. Anisimov, J. Zaanen, Phys. Rev. B 52 (1995) R5467–R5470.
[49] V.I. Anisimov, F. Aryasetiawan, J. Phys. Condens. Matter 9 (1997) 767–808.
[50] S.L. Dudarev, A.I. Liechtenstein, M.R. Castell, G.A.D. Briggs, A.P. Sutton, Phys. Rev. B 56 (1997) 4900–4908.
[51] S.L. Dudarev, G.A. Botton, S.Y. Savrasov, C.J. Humphreys, A.P. Sutton, Phys. Rev. B 57 (1998) 1505–1509.
[52] H.J. Monkhorst, J.D. Pack, Phys. Rev. B 13 (1976) 5188–5192.
[53] K. Reuter, M. Scheffler, Phys. Rev. B 65 (2001) 035406.
[54] X.G. Wang, W. Weiss, S.K. Shaikhutdinov, M. Ritter, M. Petersen, F. Wagner, R. Schlogl, M. Scheffler, Phys. Rev. Lett. 81 (1998) 1038–1041.
[55] W. Bergermayer, H. Schweiger, E. Wimmer, Phys. Rev. B 69 (2004) 195409.
[56] N.C. Wilson, S.P. Russo, Phys. Rev. B 79 (2009) 094113.
[57] J.M.D. Coey, G.A. Sawatzky, J. Phys. Chem. 4 (1971) 2386–2407.
[58] Y. Sato, S. Akimoto, J. Appl. Phys. 50 (1979) 5285.
[59] D.A. Tompsett, M.S. Islam, J. Phys. Chem. C 118 (2014) 25009–25015.